The Antarctic Circumpolar Current between the Falkland Islands and South Georgia

MICHEL ARHAN

Laboratoire de Physique des Océans, CNRS/IFREMER/UBO, Plouzané, France

ALBERTO C. NAVEIRA GARABATO AND KAREN J. HEYWOOD

School of Environmental Sciences, University of East Anglia, Norwich, United Kingdom

DAVID P. STEVENS

School of Mathematics, University of East Anglia, Norwich, United Kingdom

(Manuscript received 6 February 2001, in final form 19 November 2001)

ABSTRACT

Hydrographic and lowered acoustic Doppler current profiler data along a line from the Falkland Islands to South Georgia via the Maurice Ewing Bank are used to estimate the flow of circumpolar water into the Argentine Basin, and to study the interaction of the Antarctic Circumpolar Current with the Falkland Plateau.

The estimated net transport of 129 ± 21 Sv (Sv ≡ 10^6 m^3 s^{-1}) across the section is shared between three major current bands. One is associated with the Subantarctic Front (SAF; 52 ± 6 Sv), and the other two with branches of the Polar Front (PF) over the sill of the Falkland Plateau (44 ± 9 Sv) and in the northwestern Georgia Basin (45 ± 9 Sv). The latter includes a local reinforcement (~20 Sv) by a deep anticyclonic recirculation around the Maurice Ewing Bank. While the classical hydrographic signature of the PF stands out in this eastbound branch, it is less distinguishable in the northbound branch over the plateau. Other circulation features are a southward entrainment of diluted North Atlantic Deep Water from the Argentine Basin over the eastern part of the Falkland Plateau, and an abyssal anticyclonic flow in the western Georgia Basin, opposite to what was generally assumed.

The different behavior of the SAF and PF at the Falkland Plateau (no structural modification of the former and partitioning of the latter) is attributed to the PF being deeper than the sill depth on the upstream side of the plateau, unlike the SAF. It is suggested that the partitioning takes place at a location where the 2500-m and 3000-m isobaths diverge at the southern edge of the plateau. The western branch of the PF crosses the plateau at a distance of ~250 km to the east of the SAF. Comparison with a section across the Falkland Current farther downstream shows that its deep part subsequently joins the SAF on the northern side of the plateau where the 2000–3000 m isobaths converge in the steep Falkland Escarpment. The result of this two-stage bathymetric effect is a net transfer of at least 10 Sv from the PF to the SAF at the crossing of the Falkland Plateau.

1. Introduction

Downstream of Drake Passage, the northern part of the Antarctic Circumpolar Current describes an equatorward loop to about 40°S in the southwestern Argentine Basin before resuming its eastward course across the Atlantic (Orsi et al. 1995). This circulation feature is important as a privileged site of water exchange between the Southern Ocean and the subtropical basins. Owing to these transfers occurring primarily at the confluence of the Falkland and Brazil Currents on the northern side of the loop, most studies carried out in this region have dealt with aspects of the confluence, including its vertical structure and latitudinal variations, the associated high mesoscale variability, and the local water mass transformations. Farther south, the interaction of the fronts of the Antarctic Circumpolar Current with the complicated bathymetry that separates the Scotia Sea from the Argentine Basin (Fig. 1), though being another key process for the northward loop, has been the object of less systematic investigation. Peterson and Whitworth (1989) suggested that the Subantarctic Front (SAF) and Polar Front (PF), the two major velocity bands of the circumpolar current, cross the Falkland Plateau to the west of the Maurice Ewing Bank, with the former subsequently flowing northwestward along the Patagonian continental slope, and the latter turning eastward to the north of the bank. Peterson (1992) emphasized the large volume transport (60 Sv–70 Sv: Sv ≡ 10^6 m^3 s^{-1}) that the Antarctic Circumpolar Current contributes to the Falkland Current, thus revealing the importance of the overflow of southern waters at the

Corresponding author address: Michel Arhan, Laboratoire de Physique des Oceans, CNRS/IFREMER/UBO, IFREMER/Brest, B.P. 70, Plouzane 29280, France.
E-mail: marhan@ifremer.fr

Falkland Plateau and the typical intensity of the northward loop. The large transport was corroborated by subsurface float measurements between Drake Passage and the Argentine Basin by Davis et al. (1996). A still unsettled point, however, concerns the exact pathway of the Polar Front in the vicinity of the Maurice Ewing Bank. Moore et al. (1997), from satellite sea surface temperature data, and Trathan et al. (2000) using a hydrographic transect to the northwest of South Georgia, locate the Polar Front to the south of the bank, at variance with the above-quoted result of Peterson and Whitworth (1989).

In this paper, we describe and quantify the flow of Drake Passage water toward the north and northeast between the Falkland Islands and South Georgia, using full-depth hydrographic and lowered acoustic Doppler current profiler (L-ADCP) measurements collected during the British cruise ALBATROSS (Fig. 1). The quasi-zonal part of the cruise track between the Falkland Islands and the Maurice Ewing Bank samples the complete Falkland Plateau overflow. The line from the bank to South Georgia intersects the Polar Front signatures observed by Moore et al. (1997) and Trathan et al. (2000). At depth, it samples the Weddell Sea waters that occupy the abyss of the Georgia Basin (Whitworth et al. 1991).

After a description of the hydrographic structure in section 2, we present the L-ADCP and geostrophic cross-track velocities in section 3. The circulation patterns and associated transports are discussed in sections 4 and 5, respectively. In section 6, we compare the overflow results with estimates of the Falkland Current transport from the World Ocean Circulation Experiment (WOCE) hydrographic line A17 (Fig. 1), and question the possible role of this region for the injection of North Atlantic Deep Water (NADW) into the circumpolar current.

2. The data and distributions of hydrographic parameters

The ALBATROSS stations (124 to 170) shown in Fig. 1 are part of a larger box-shaped hydrographic and tracer survey around the Scotia Sea that was aimed at describing the pathways and property changes of the circumpolar and Weddell Sea waters in this oceanic basin. This full-depth survey was conducted during cruise 40 of the RRS *James Clark Ross,* from 15 March to 22 April 1999. A description of the cruise and data processing may be found in Heywood and Stevens (2000). The subset of data used in this paper (collected from 14 to 22 April) has a station spacing between 34 km and 48 km except over the continental slope of South Georgia, where successive stations were located to have bottom depth variations of less than 500 m. In the following, we refer to the nearly zonal portion of the survey (stations 142–170) as the Falkland Plateau line. The section from South Georgia to the Maurice Ewing Bank (stations 124–142) is referred to as the Georgia Basin line.

a. The water masses

The water mass distributions along the entire ALBATROSS survey were discussed by Naveira Garabato et al. (2002, hereafter NGHS). As reference for the presentation of the volume transports the vertical distributions of potential temperature, salinity, and dissolved oxygen between the Falkland Islands and South Georgia are shown in Fig. 2. Figure 3 gives the corresponding full-depth and deep potential temperature–salinity (θ–S) diagrams. Superimposed on these figures, and reported in Table 1, are the isopycnal surfaces selected to separate the different water masses. These separations are quasi-identical to those observed by Sievers and Nowlin (1984) in Drake Passage except for an additional one ($\sigma_2 = 37.04$)[1] used to subdivide the Lower Circumpolar Deep Water (LCDW) as in Arhan et al. (1999).

From top to bottom, we first distinguish the Antarctic Intermediate Water (AAIW; $\sigma_0 < 27.35$), in which we include the 4°–5°C thermostad of the Subantarctic Mode Water visible at the western end of the section (Figs. 2a,b), and a small volume of surface water. Below AAIW, the Upper Circumpolar Deep Water (UCDW) is characterized by a pronounced oxygen minimum at $27.35 < \sigma_0$, $\sigma_2 < 36.98$ (Fig. 2d). Farther down, the layer $36.98 < \sigma_2 < 37.11$ of LCDW corresponds approximately to the domain of salinity higher than 34.7 (Fig. 2c). At the western end of this layer (inshore of station 161), a small amount of LCDW is present in the domain of shoreward deepening isopleths that characterize the SAF. The density range $36.98 < \sigma_2 < 37.04$ of this water coincides with that of a separate core of high velocity in the Falkland Current described by Arhan et al. (1999). Following those authors, we subdivide the LCDW in two sublayers, namely the LCDW-1 ($36.98 < \sigma_2 < 37.04$) and the LCDW-2 ($37.04 < \sigma_2 < 37.11$). The separating density (equivalent to $\sigma_4 = 45.87$ and here defined as the highest density found in the SAF) happens to be close to the lower limit of influence of the NADW in the Argentine and Brazil Basins (e.g., Durrieu de Madron and Weatherly 1994). In Fig. 2c, several patches of high salinity ($S > 34.72$ psu) are observed in the LCDW layer over the sill of the Falkland Plateau and on either side of the Maurice Ewing Bank. As some of these peak values exceed the highest salinities in Drake Passage, NGHS attributed them to an influence of the NADW present in the Argentine Basin. In Fig. 3b this interpretation is supported by these higher values (associated with strong interleaving) being mostly found at densities lower than $\sigma_2 = 37.04$, the NADW lower limit.

Another noteworthy observation in Fig. 2 is the near

[1] The potential density unit (kg m^{-3}) is omitted in the paper.

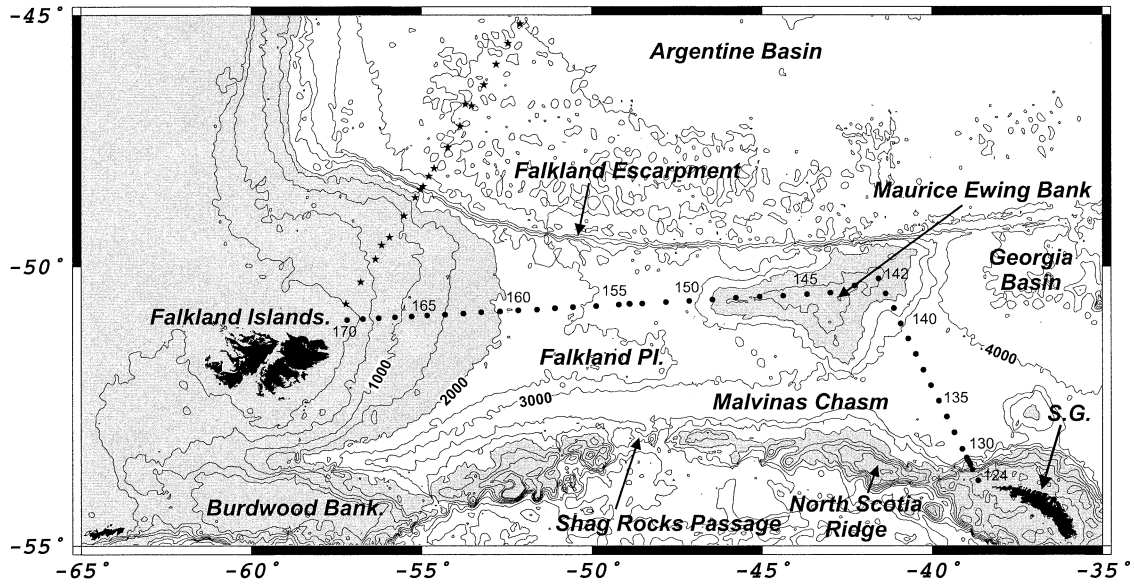

FIG. 1. Bathymetric configuration in the region between the Falkland Islands and South Georgia (S.G.). Isobaths 200 m, multiples of 500 m (down to 3000 m), and multiples of 1000 m (below 3000 m) are shown. The domain shallower than 2000 m is shaded. The ALBATROSS stations (dots) 124 to 170 are shown. The southern part of the WOCE hydrographic line A17 used to compare the overflow and Falkland Current transports, is also shown (stars).

coincidence of the lower isopycnic limit of the LCDW with the bottom of the saddle region of the Falkland Plateau. Having observed a sharp vertical density gradient at the base of the LCDW in the deep Falkland Current downstream of the ALBATROSS line, Arhan et al. (1999) suggested that the whole density range of this water mass could overflow the Falkland Plateau. This is verified here with extreme bottom water characteristics $\theta = 0.6$°C, $S = 34.70$ psu, and $\sigma_2 = 37.11$ ($\sigma_4 = 45.98$) at 47°–49°W near the sill of the plateau.

Water denser than $\sigma_2 = 37.11$ is only detected along the Georgia Basin line. In Drake Passage, Sievers and Nowlin (1984) observed that the layer $37.11 < \sigma_2$, $\sigma_4 < 46.04$ is occupied by a variety of Circumpolar Deep Water characterized by a silicate maximum, and referred to it as Southeast Pacific Deep Water (SPDW) to indicate the origin of that signal. Although their layer nomenclature is preserved in this study, NGHS noted that in much of the Georgia Basin line the properties of SPDW have been eroded by mixing with Weddell Sea waters, causing the layer characteristics to be indistinguishable from those in the northern limb of the Weddell gyre. Only at two deep stations located between 40°30′W and the edge of the Maurice Ewing Bank did they observe a remnant of the SPDW properties in Drake Passage (in Fig. 3b, slightly higher salinities denote the presence of this remnant). This SPDW core probably flows around the bank toward the Argentine Basin after exiting the Scotia Sea through Shag Rocks Passage (Fig. 1). The deepest layer $\sigma_4 > 46.04$ in the transect is occupied by Weddell Sea Deep Water (WSDW).

b. The fronts

The crossing of the depth level 200 m by the 4°C isotherm has been a widely used criterion for determining the location of the SAF (Peterson and Whitworth 1989). Using this criterion in Fig. 2a, the front is placed near 53°W (stations 161–162), at a location where the ocean depth is 2000 m as previously noted by Peterson and Whitworth (1989). In the upper 800 m the front marks the offshore limit of the 4°–5°C thermostad of the Subantarctic Mode Water, but the observation of strong lateral gradients of all parameters down to the bottom (Figs. 2b,c,d) reveals its full-depth character.

The Georgia Basin line is a partial repeat of the section used by Trathan et al. (2000) to locate the PF above the southeastern flank of the Maurice Ewing Bank. Enhanced slopes of all isopleths at longitudes 40°30′W–41°W in Fig. 2 (stations 137–139) indeed reveal the front in Figs. 2b,c,d.

To the west of the Maurice Ewing Bank in Fig. 2, two locations with eastward rising isopycnals could possibly mark a PF spatial pattern comparable to the one suggested by Peterson and Whitworth (1989). One lies at 49°–50°W (stations 154–156) near the deepest part of the plateau, and the other around 46°30′W (station 149) above the western flank of the Maurice Ewing Bank. The direct current measurements presented below will reveal the former as another major band of northward current with significant near-bottom magnitude. At the latter location, on the contrary, a southward near-bottom flow will be found counteracting the geostrophic shear. In anticipation of these results, we mark the lo-

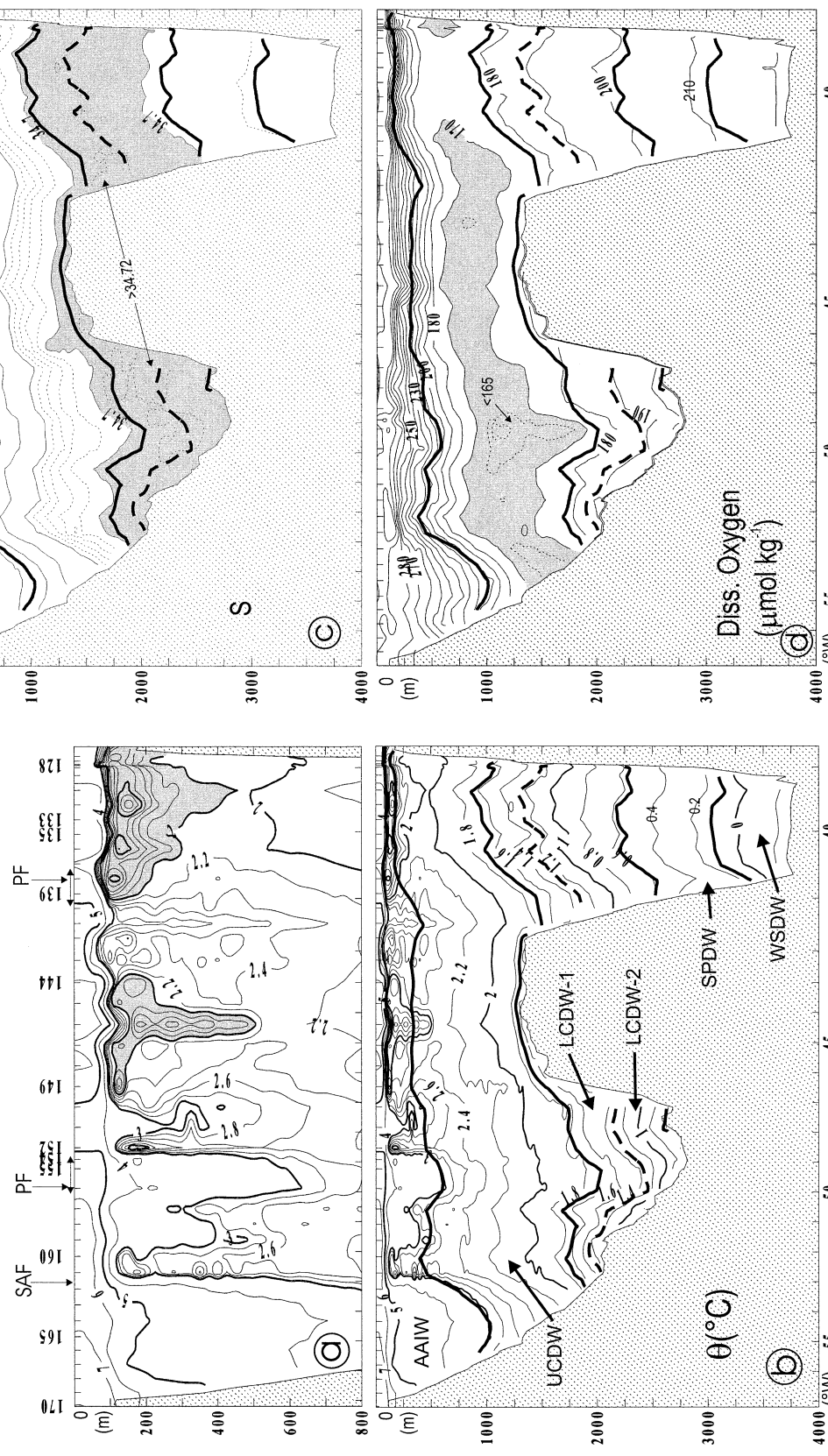

FIG. 2. Vertical distribution of water properties along the ALBATROSS line from the Falkland Islands to South Georgia: (a) and (b) potential temperature, (c) salinity, and (d) dissolved oxygen. In (b), (c), and (d), the bold lines are the water mass isopycnal limits indicated in the second column of Table 1 (the boundary between LCDW-1 and LCDW-2 is shown as a dashed line). In (a) the shaded domain $\theta < 2°C$ shows the Antarctic temperature minimum characteristic of the poleward side of the Polar Front. The shaded domains in (c) ($S > 34.7$) and (d) ($O_2 < 170$ μmol kg^{-1}) show the high salinities of the LCDW and low oxygen concentrations of the UCDW, respectively.

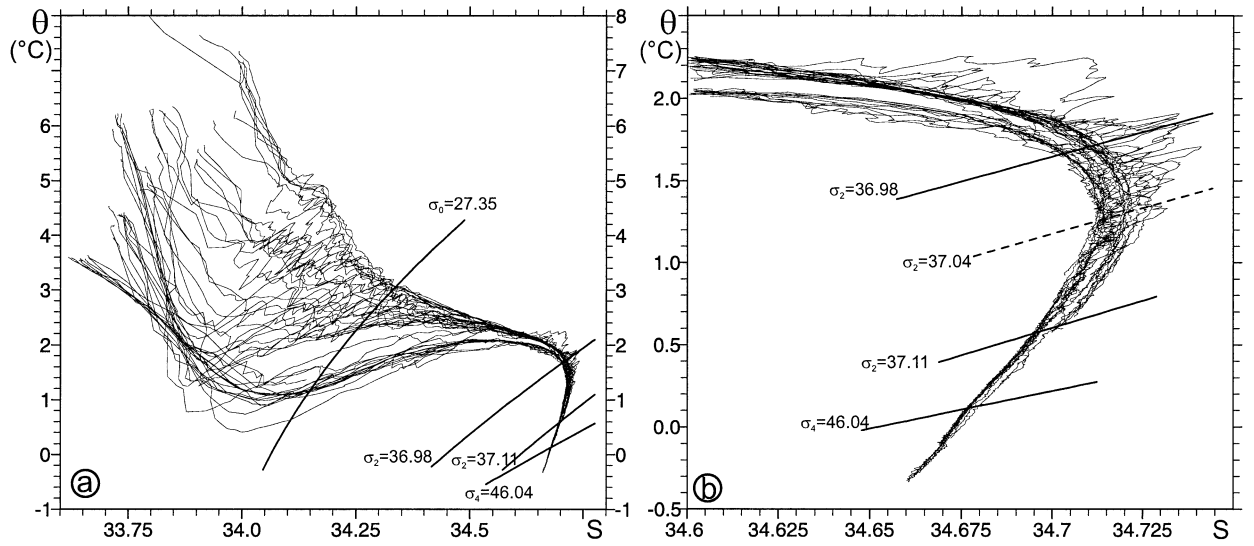

FIG. 3. Full depth (a) and deep (b) θ–S diagrams of ALBATROSS stations 124 to 170, with the water mass isopycnal limits superimposed.

cation 49°–50°W as a second branch of the PF in Fig. 2a. The isopycnal slopes observed there are weaker than to the southeast of the bank and adjacent to a reversed signal to the west. Thus, it would have been difficult to ascertain whether this is a frontal signature based solely upon hydrographic measurements.

The PF has often been recognized as the northernmost limit of a subsurface temperature minimum ($\theta < 2$°C) shallower than 200 m (Peterson and Whitworth 1989). A strict application of this criterion to Fig. 2a would indeed identify the PF with the western branch just mentioned, as a core of water colder than 2°C is present around depth 180 m at station 152. We observe, however, that the temperature minimum $\theta < 2$°C is not continuous between the two suggested main branches of the PF in Fig. 2a. Naveira Garabato et al. interpreted the discontinuities as a possible meandering of the upper part of the front above the Maurice Ewing Bank.

Gordon et al. (1977) pointed out that the SAF and PF can also be detected in the θ–S space as gaps separating otherwise clustered sets of stations. We indeed recognize the SAF around $\theta = 5$°C, $S = 34.0$ psu and the eastern PF branch around $\theta = 2$°C, $S = 34.25$ psu in Fig. 3a but, due to the discontinuity of the shallow temperature minimum to the west of 41°W, the western PF branch is not visible.

TABLE 1. Isopycnal limits of the water mass layers used in the paper. The correspondence with the neutral density limits used by Naveira Garabato et al. is given in the fourth and fifth columns.

Water mass	Potential density limits		Neutral density limits	
	Upper	Lower	Upper	Lower
AAIW	Surface	$\sigma_0 = 27.35$	Surface	27.55
UCDW	$\sigma_0 = 27.35$	$\sigma_2 = 36.98$	27.55	28.00
LCDW-1	$\sigma_2 = 36.98$	$\sigma_2 = 37.04$	28.00	28.09
LCDW-2	$\sigma_2 = 37.04$	$\sigma_2 = 37.11$	28.09	28.20
SPDW	$\sigma_2 = 37.11$	$\sigma_4 = 46.04$	28.20	28.26
WSDW	$\sigma_4 = 46.04$	Bottom	28.26	Bottom

3. Velocities

The L-ADCP profiles were obtained using an RDI 150-Hz broadband instrument fitted centrally in the CTD rosette frame. The details of the operational procedure and data processing are discussed by Heywood and Stevens (2000). The instrument was set to water and bottom tracking mode, and the velocity averaged in 20-m bins. In water tracking mode, the barotropic flow was estimated from the on-station ship displacements deduced from differential GPS data, and the contribution of tidal velocities was removed using a tidal model (Egbert et al. 1994). To estimate the accuracy of the measurements, the mean difference between water-tracking and bottom-tracking velocities (over their common depth range) was plotted at each station against the mean difference between water-tracking and shipborne ADCP velocities. The resulting scatterplot had a root mean square radius of 4 cm s^{-1}, which was considered a typical measure of the accuracy of the L-ADCP velocities. The L-ADCP velocity vectors averaged over each water mass layer are displayed in Fig. 4, and the vertical distribution of the cross-track component is shown in Fig. 5a.

The currents associated with the Antarctic circumpolar fronts are known to have significant barotropic components that hinder the determination of their absolute transports from hydrographic measurements. Here we determined a second estimate of the cross-track velocity from a least squares fitting of the geostrophic shear velocities onto the L-ADCP profiles. As an illustration, Fig. 6 shows the adjusted geostrophic profile

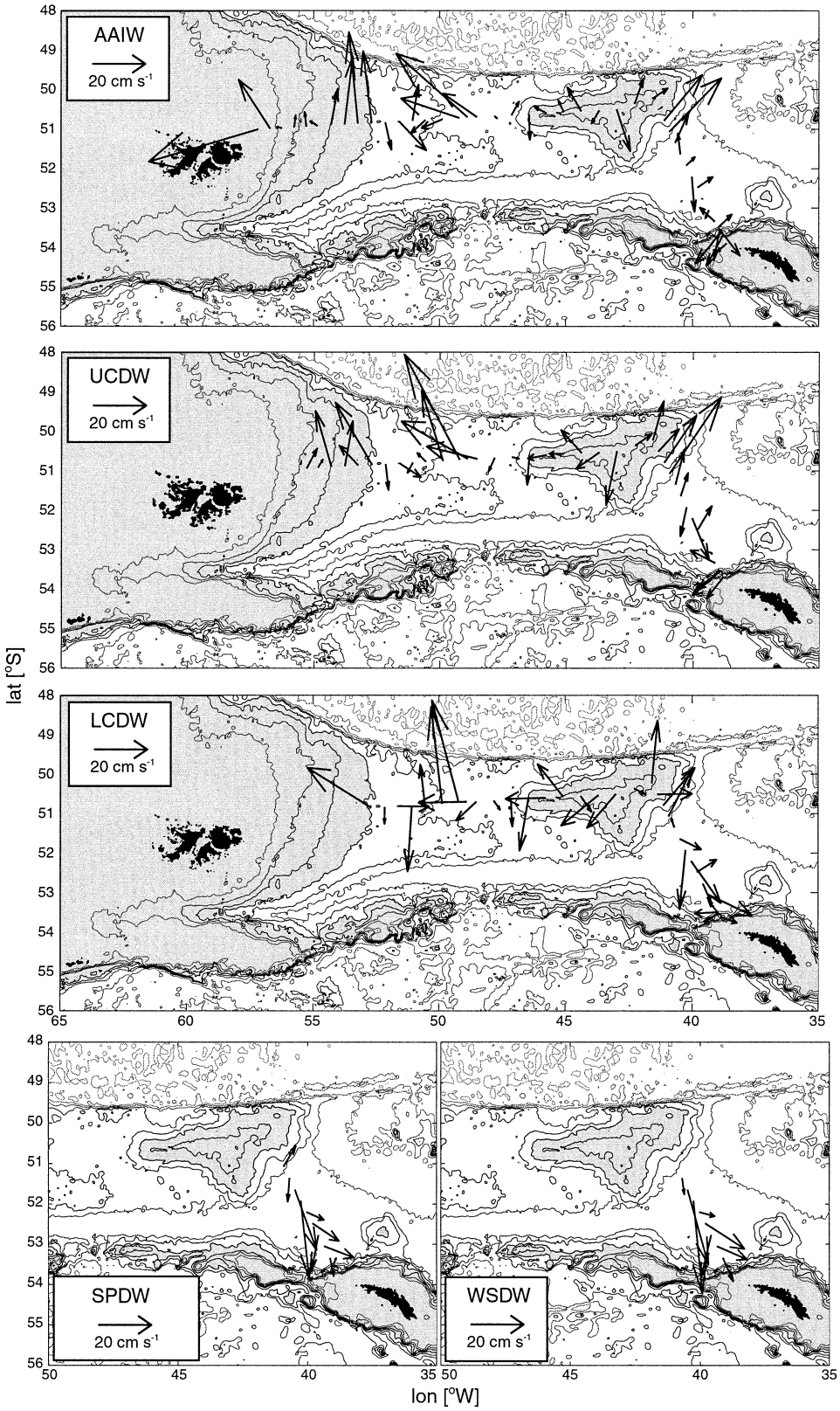

FIG. 4. L-ADCP velocity vectors at the ALBATROSS stations, averaged vertically over the water mass layers. Isobaths multiples of 500 m (down to 3000 m) and multiples of 1000 m (below 3000 m) are shown. The domain shallower than 2000 m is shaded.

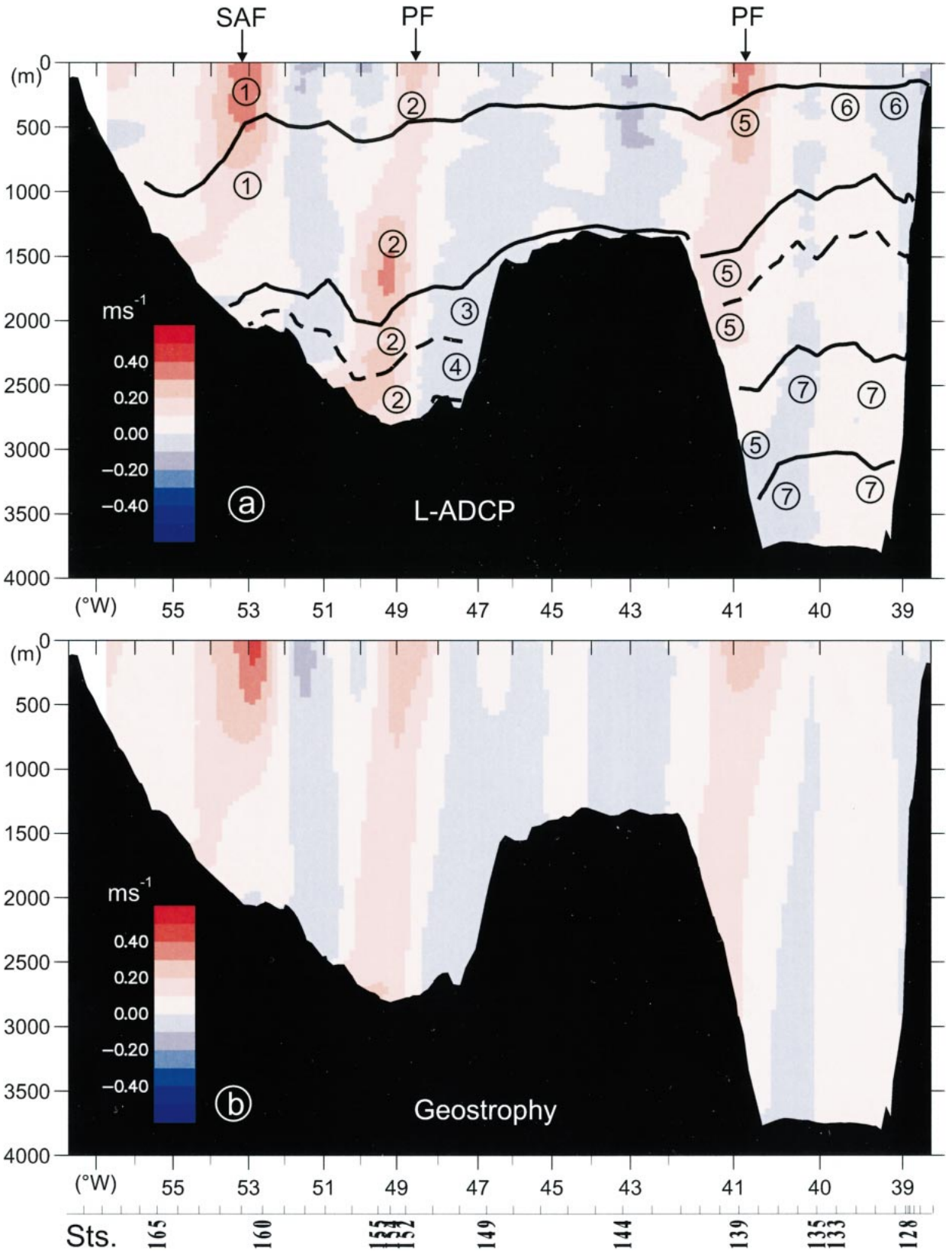
SAF
PF
PF
(m)
0
500
1000
1500
2000
2500
3000
3500
4000
ms-1
0.40
0.20
0.00
−0.20
−0.40
a
L-ADCP
(°W)
55
53
51
49
47
45
43
41
40
39
b
Geostrophy
Sts.
165
160
155
154
152
149
144
139
135
133
128

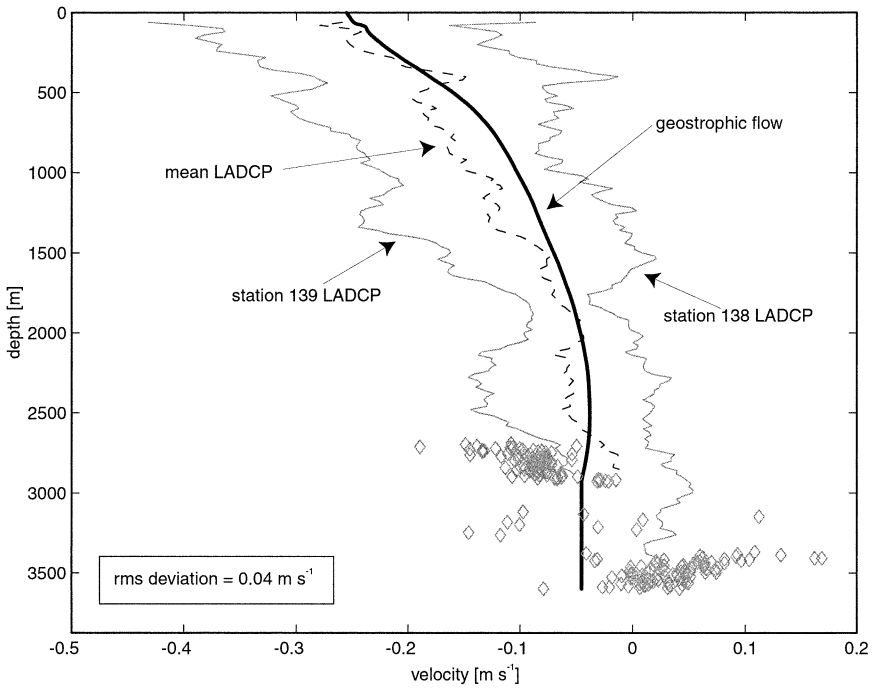

FIG. 6. Illustration of the adjustment of the geostrophic velocity shear onto the L-ADCP velocity profiles, for station pair 138–139. The figure shows the L-ADCP velocity profiles at the two stations (continuous thin lines), the resulting averaged profile (broken line), and the adjusted geostrophic profile (bold continuous). Diamonds show the L-ADCP velocity values in the bottom-track mode.

and the reference L-ADCP profile for a station pair located in the PF eastern branch. The adjustment was generally satisfactory, with an averaged root mean square deviation of about 3 cm s^{-1} over all station pairs. The vertical distribution of the adjusted geostrophic velocities in Fig. 5b confirms the general agreement with the L-ADCP velocities (Fig. 5a). Both Figs. 5a and 5b display prominent currents associated with the SAF (52°–54°W) and the PF eastern branch (40°30′–41°W), which were clearly visible in Fig. 2. Here there is also a third column of high velocity around 49°30′W that was not so obvious in that figure. Within this feature, station pair 155–156 centered at 49°30′W is by far the one that showed the least satisfactory adjustment of the geostrophic shear on the L-ADCP profile, with a root mean square deviation of 10 cm s^{-1}. In Fig. 5a this manifests itself as an ~0.4 m s^{-1} velocity core at depth 1500–2000 m, which is not present in Fig. 5b. We have good reasons to believe in the reality of this feature, as it is present in two stations and corresponds to a pronounced core of low oxygen values (<165 μmol kg^{-1}) in Fig. 2d. Its absence in the geostrophic profile might result from a strong veering of this current branch at this location, as visible in the UCDW and LCDW panels of Fig. 4, and a possibly significant cyclostrophic velocity component. In Fig. 4, this veering seems dictated by a neighbouring acute angle of the 2500-m isobath. In order to produce the observed 15 cm s^{-1} difference between the geostrophic and L-ADCP velocities, a radius of order 10 km would be required for the flow curvature.

4. Water mass circulation patterns

In this section we discuss the main water mass pathways that can be inferred from Figs. 4 and 5. A schematic of the pathways is presented in Fig. 7 using the identifying numbers reported on the velocity distribution of Fig. 5a to visualize the layers concerned.

a. The SAF route

The path of the SAF shown in Fig. 7 (path number 1) is a simplified version of the one determined by Peterson and Whitworth (1989), with a crossing of the North Scotia Ridge at the gap 2000 m deep located to

←

FIG. 5. (a) Vertical distribution of the L-ADCP velocity component normal to the ALBATROSS line (positive northward and northeastward). Superimposed are the water mass limits and the numbers identifying the pathways of Fig. 7, to show the depth range affected by each route. (b) Vertical distribution of geostrophic velocities referenced to the L-ADCP velocities using a least squares procedure.

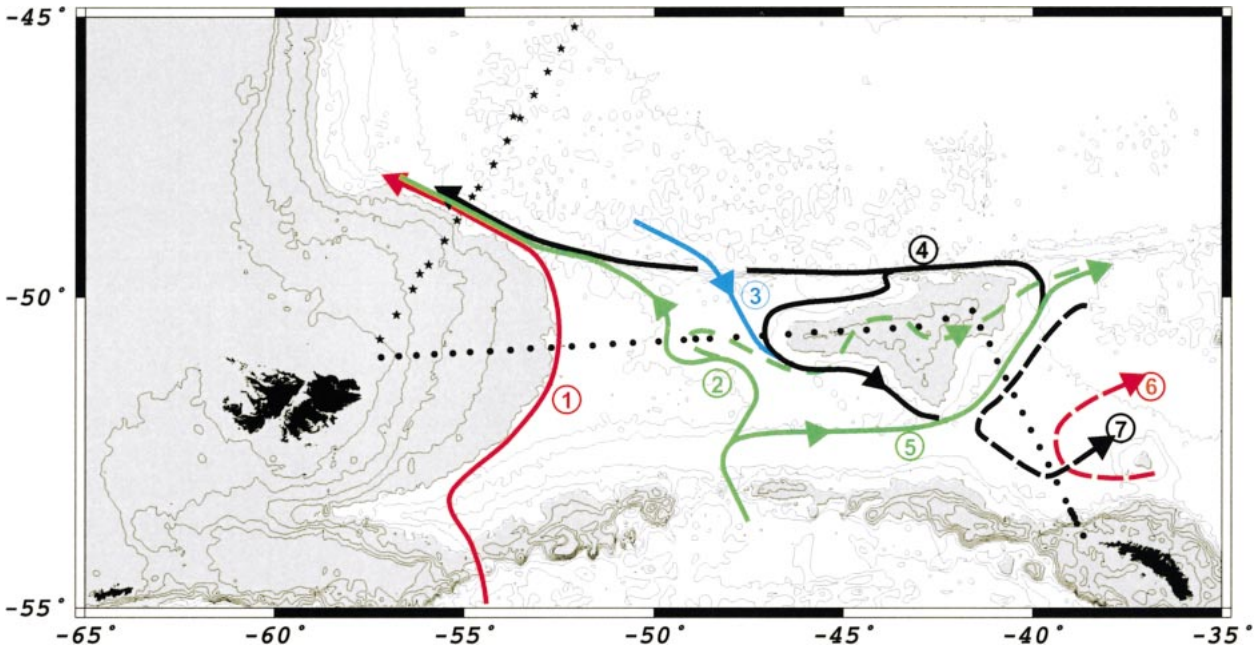

FIG. 7. Schematized main water-mass pathways discussed in the text. The path numbers are those of Fig. 5a. The red line (1) is the SAF route, the green lines (2) and (5), and the unnumbered dashed line above the Maurice Ewing Bank, show the behavior of the PF. The blue line (3) represents the flow carrying diluted NADW southward over the eastern part of the plateau. The black line (4) shows the westward path of SPDW along the Falkland Escarpment and an anticyclonic circulation of LCDW around the bank. Lines (6) (dashed red) and (7) (dashed black) represent the opposed upper and deep circulations across the Georgia Basin line. Isobaths are identical to those of Fig. 1.

the east of Burdwood Bank (Fig. 1) and a subsequent alignment with the 2000-m isobath. This current conveys water up to density $\sigma_2 = 37.04$, which was chosen above as a separation between LCDW-1 and LCDW-2.

In Drake Passage, NGHS pointed out the presence of two distinct types of Circumpolar Deep Water in the approximate density range of the UCDW and LCDW-1. Beside the dominant type, which occupies most of the breadth of the passage, an anomalous low-oxygen type ($O_2 < 160$ μmol kg^{-1}) arriving from along the Chilean continental slope was observed inshore of the SAF and at a few stations on the equatorward flank of the PF. The anomalous UCDW is again recognized here (Fig. 2d) from its low oxygen signature ($O_2 < 165$ μmol kg^{-1}) between the SAF and the continental slope, obviously following this front beneath the AAIW.

b. A branching of the Polar Front

The PF pattern suggested by the ALBATROSS data is more complicated than the SAF one. The current band at 40°30′–41°W over the southeastern flank of the Maurice Ewing Bank affects the AAIW, UCDW, LCDW, and the core of SPDW present against the slope at this location. At 48°–51°W, the third column of intense northward velocity in Fig. 5a raises the question of a possible branching of the front. Several reasons suggest that this current column results from a lateral and, to some extent, vertical splitting of the PF. First, although a trough in the isopycnals and another core of anomalous UCDW ($O_2 < 165$ μmol kg^{-1}) at 49°–50°W could be indicative of an eddylike structure, the strong northward bias of the velocity profiles in this region (Fig. 4) is definitely that of a front, not of an eddy. The only significant deep southward velocities are found in the LCDW layer on the western side of the front, where a U-shaped salinity pattern in Fig. 2c also suggests a recirculating component. However these southward velocities have magnitudes less than one third of the northward flow. Another clue in support of a PF branching is the density value ($\sigma_2 = 37.11$ or $\sigma_4 = 45.98$) of the bottom water in the current band. Arhan et al. (1999) noted that this isopycnal, here observed at the ~2800 m deep saddle of the plateau, is only found at such depths within or south of the PF in Drake Passage, being some 800 m deeper to the north of the front. Our finding of such a bottom density at station 155 at the eastern edge of the central current band therefore strongly suggests that this current is the (detached) northern part of the PF.

The two PF branches inferred from the above analysis are the lines numbered 2 and 5 in Fig. 7. Although both are full-depth current bands, Fig. 5a reveals their different vertical structures. The upper-ocean intensification of the eastern branch, and the contrasting highest velocities below 1500 m in the western one, betray an unequal vertical sharing of kinetic energy at the splitting of the initial current column. That the deeper velocity core (the western branch) follows the shallower path over the Falkland Plateau while the shallower velocity core (the eastern branch) proceeds toward the deeper

Georgia Basin probably reflects an upward weakening of the topographic steering effect causing the bifurcation. The pronounced poleward shallowing of isopycnals associated with the eastern branch is qualitatively similar to the PF structure in Drake Passage. In previous studies, this may have favored the detection of this branch from hydrographic measurements alone. The different hydrographic structure of the western branch impedes its recognition as a PF bifurcation. This branch is only detected here due to the direct current measurements. In the schematics of the PF by Peterson and Whitworth (1989, their Fig. 4) and Moore et al. (1997, their Plate 2), the current is seen to cross the Malvinas Chasm to the north of Shag Rocks Passage (Fig. 1) in a nearly meridional direction. Having reproduced this behavior in Fig. 7, we observe that the current should then reach the Falkland Plateau near 52°S–47°30′W, at a location where the isobaths 2500 m and 3000 m strongly diverge. As such bathymetric configurations are favorable to current branching (Warren 1969), we placed the bifurcation at this location in Fig. 7. The effect of the Falkland Plateau on the PF looks similar, in some respects, to that of the Kerguelen Plateau in the Indian sector of the circumpolar current, as described by Sparrow et al. (1996). These authors also found a splitting of the front, with a branch flowing over a col in the plateau and another skirting the bathymetry.

We pointed out above that shallow hydrographic signatures typical of the poleward side of the PF suggest a meandering of this structure between the two major branches. The alternate velocity columns observed at 42°–48°W (Fig. 5a) are compatible with such a flow pattern, and suggest that it would affect the UCDW as well as the AAIW. In Fig. 7 we tentatively represent the meanders by the dashed (unnumbered) line between branches 2 and 5. As seen in this figure, this third (shallow) branch of the front requires a second bifurcation of branch 2 at a short distance downstream of the separation from branch 5. When considering possible reasons for this second branching, we note that the upper part of branch 2 is probably less constrained by the bathymetry than the lower part. This may be sufficient to explain its partial entrainment by an adjacent deeper southward flow (branch 3 in Fig. 7). The presence of the shallow meandering branch of the PF matches the finding of a PF pathway to the west and north of the Maurice Ewing Bank by some authors (Peterson and Whitworth 1989; Orsi et al. 1995) based on the shallow temperature minimum ($\theta < 2$°C) criterion.

c. An anticyclonic flow around the Maurice Ewing Bank

Whitworth et al. (1991) analyzed 14-month velocity records from an array north of the Maurice Ewing Bank along 41°W. They found that, on average, a narrow deep westward boundary current exists against the northern flank of the bank, particularly intensified (20–30 cm s^{-1} average velocity) at depths 1500–3500 m, and still significant (10 cm s^{-1}) near the 5500-m-deep bottom. Their result, along with our snapshot observations (Fig. 5a) of northeastward and southward flows on the southeastern and western sides of the bank, respectively, are evidence of a deep anticyclonic flow around the bathymetry.

From Fig. 7, the eastbound branch of the PF (numbered 5) constitutes the southeastern limb of the anticyclonic flow. Within this branch, the LCDW and SPDW layers, which are deeper than the summit of the bank (Fig. 5a), should be more constrained by the bathymetry than the UCDW and AAIW above. In the boundary flow to the north of the bank revealed by the study of Whitworth et al. (1991), the vertical intensification of the currents indeed occurs at potential temperatures of 0.2° to 1.8°C (their Fig. 3), the approximate range of the LCDW and SPDW (Fig. 2b). The core of SPDW, being denser than the deepest water at the saddle of the Falkland Plateau, is compelled to proceed westward along the Falkland Escarpment as a deep component of the Falkland Current (pathway 4 and its westward extension in Fig. 7).

As the density range of the LCDW is present to the west of the Maurice Ewing Bank over the sill of the plateau, there is no bathymetric obstacle to prevent a fraction of this water mass from performing a complete circuit around the bank, provided that the bathymetric guidance is sufficient. In the LCDW-2 sublayer not influenced by the NADW, we verified that the deep θ–S diagrams in the near-bottom southward flow to the west of the bank (region 4 at 47°–48°W in Fig. 5a) are identical to those of the same layer in branch 5 above the southeastern slope. This confirms the closed recirculation of some LCDW around the bank, as represented in Fig. 7.

A closed recirculation also most certainly exists in the LCDW-1 layer, yet with some alteration of the water properties to the west of the bank where the anticyclonic flow entrains diluted NADW from the Argentine Basin (Figs. 2c, 3). Peterson and Whitworth (1989) noted the presence of some NADW at depth in the eastward Falkland Return Current that flows adjacent to the opposing Falkland Current at longitudes 50°–55°W. They observed that this NADW may occasionally be entrained back westward along the continental slope by the boundary flow. Here we provide evidence of a southward entrainment of a part of the deep Falkland Return Current over the eastern part of the Falkland Plateau (pathway number 3 in Fig. 7), and of its subsequent incorporation in the eastbound branch of the PF. As a proof of this flow, we trace the NADW from its expected high salinity anomaly and low values of the quasi-conservative tracer PO_4^* (see Broecker et al. 1998), defined as $PO_4^* = PO_4 + O_2/175 - 1.95$ μmol kg^{-1}. Figure 8 shows the deep PO_4^*–S scatterplots of stations 150 and 141, located above the slope on either side of the bank, along with those of the PF in Drake Passage. In the latter, the

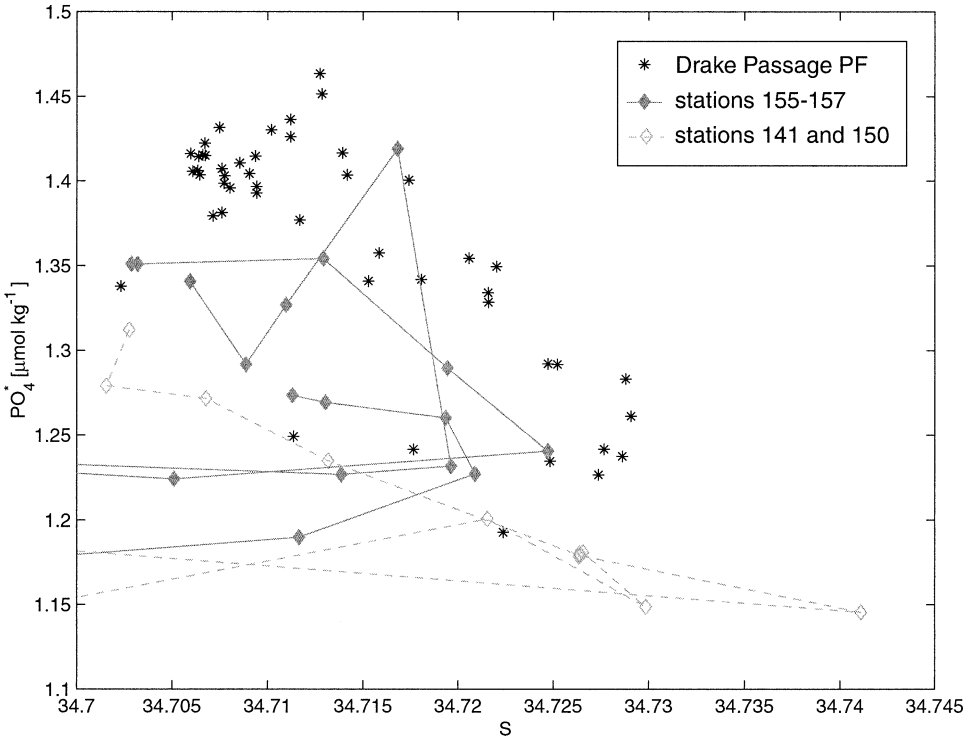

FIG. 8. PO_4^*–*S* diagrams of stations 141, 150, and 155–157 (diamonds), for detection of the NADW influence by comparison with other ALBATROSS stations in the PF in the Drake Passage (stars).

LCDW salinity maximum is close to 34.73 psu, with associated PO_4^* values between 1.25 and 1.3 μmol kg^{-1}. Above the western slope of the Maurice Ewing Bank, the presence of NADW in the southward-flowing water sampled at station 150 is detected by both a higher salinity maximum (34.741 psu) and a lower PO_4^* value (1.15 μmol kg^{-1}). On the other side of the bank, the reduced salinity maximum of 34.73 psu at station 141 is not in itself an absolute proof of the NADW influence, but the associated PO_4^* value of 1.15 μmol kg^{-1}, clearly lower than in Drake Passage, is an unambiguous signature of the merging of pathway 3 in the PF branch 5. Finally, Fig. 8 also shows the PO_4^*–*S* diagrams of stations 155–157 that sampled the other, U-shaped, high salinity pattern in the LCDW layer (Fig. 2c). Unlike those of stations 150 and 141, these diagrams show no trace of a NADW influence in the PF branch 2 above the sill of the plateau.

d. Circulation patterns in the western Georgia Basin

Along the Georgia Basin line, NGHS emphasized the different properties of the waters sampled to the west of 40°30′W (in the PF branch number 5), relative to those found farther east. They related the dissimilarity to the different routes followed by the waters from the Scotia Sea to the western Georgia Basin. While the PF takes the shortest path through Shag Rocks Passage and the Malvinas Chasm (Fig. 1), the waters farther to the southeast enter the Georgia Basin after skirting South Georgia. Having already discussed the PF branch above, we now focus on the waters observed east of 40°30′W. From Fig. 5a, two dominant regimes are found in the vertical, which we illustrate by pathways 6 and 7 in Fig. 7.

Above depth about 1500 m ($\sigma_2 \approx 37.04$ psu), the flow is westward against the continental slope of South Georgia and eastward farther offshore to about 40°W. This suggests a cyclonic flow at these depths in the southern half of the Georgia Basin line, as represented by pathway number 6, with a change of direction at 39°22′W (station 131) where a doming of the isotherms and isopycnals is observed below 500 m (Fig. 2b). Orsi et al. (1995) showed that, in addition to the SAF and PF, the Antarctic Circumpolar Current is associated with a third deep-reaching and more southern front, which they called the Southern Antarctic Circumpolar Current Front (SACCF). This feature can be identified from a value of the UCDW temperature maximum between 1.8° and 2°C at a depth near 500 m. In the frontal patterns determined by Orsi et al. (1995), the SACCF makes a northwestward loop in the Georgia Basin with a narrow cyclonic westward protrusion north of South Georgia. Although the cyclonic pathway 6 in Fig. 7 is probably influenced by this frontal pattern, the front itself was not intersected by the Georgia Basin line. This we conclude from the observation that the UCDW temperature maximum remains higher than 2°C at the location of flow reversal (station 131; Fig. 2a). In a study of the

SACCF variability in this region, Thorpe et al. (2001, manuscript submitted to *J. Mar. Syst.*) indeed found that the western tip of the protrusion is located on average near 36°W, some 250 km to the east of the Georgia Basin line.

Underneath the PF branch number 5, the flow direction reverses to an anticyclonic pattern below about $\sigma_2 = 37.04$ (pathway 7 in Fig. 7). Given the full-depth doming of the isopycnals along the Georgia Basin line, and the generally barotropic character of the Antarctic Circumpolar Current, such a reversal in the vertical was not expected. Several previous studies indeed regarded the doming of the abyssal isotherms as the signature of a cyclonic circulation (Georgi 1981; Orsi et al. 1993; Arhan et al. 1999). The opposite flow observed during ALBATROSS may not be stationary, as Whitworth et al. (1991) emphasized the marked temporal variability of the abyssal flow in this region; nor does it necessarily apply to the whole area of the western Georgia Basin. However, the different locations of westward flow across the Georgia Basin line, that is, against the North Scotia Ridge in the upper layers and against the Maurice Ewing Bank near the bottom, might be related to separate inflows into the western Georgia Basin. While the upper-water inflow occurs along the SACCF above the northern flank of the North Scotia Ridge, the near-bottom supply can only take place to the north of 50°S, equatorward of the Northeast Georgia Rise, a bathymetric obstacle located at 50°–54°S, 32°–35°W just outside the maps of Figs. 1 and 7.

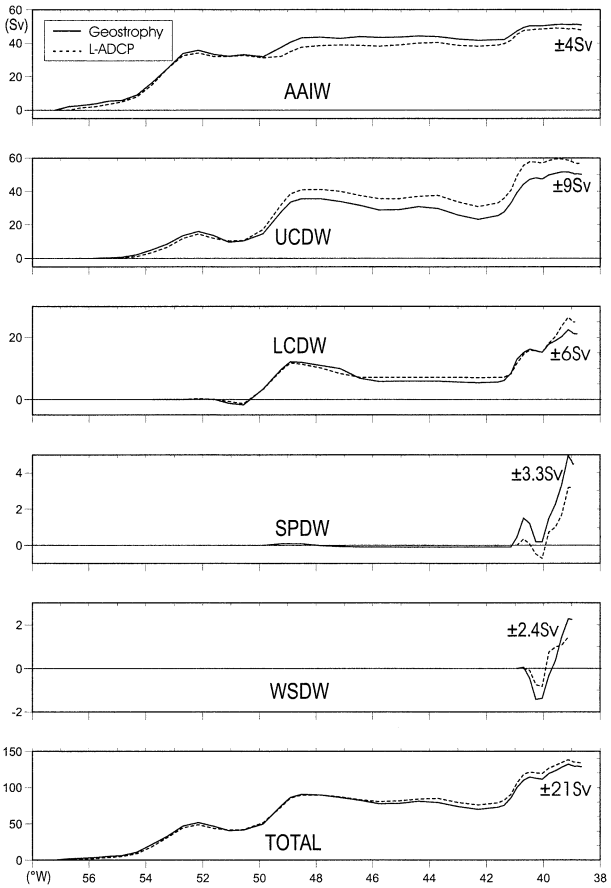

FIG. 9. Geostrophic and L-ADCP volume transports across the ALBATROSS line, accumulated eastward from the Falkland Islands, for each water mass and the total water column. The uncertainties reported in each panel were estimated as indicated in the text.

5. Transports

The adjusted geostrophic and L-ADCP volume transports across the hydrographic line, accumulated eastward from the shelf of the Falkland Islands, are displayed in Fig. 9 for each water mass and the whole water column. The agreement between the two curves of each Figure panel is generally satisfactory, a confirmation that the vertical shears of the geostrophic and L-ADCP velocities are comparable. There are, however, a few local divergences, particularly near 49°W, a consequence of the aforementioned disparity of the two velocity shears at station pair 155–156. The along-track integrated discrepancies range from 0.8 Sv in the WSDW to 6 Sv in the UCDW.

In the above we gave an error estimate of ± 4 cm s^{-1} for the L-ADCP velocity measurements. With this uncertainty as a starting point, estimating error bars for the transports remains difficult, because of a lack of information on possible vertical and lateral correlations of the velocity errors. We assumed a perfect vertical correlation, that is, error-free vertical shears, and a total independence of the velocity errors at different station pairs. Further, assuming a normal distribution N(0., 4 cm s^{-1}) for the latter, we generated a large number (100) of modified cross-track transport estimates and calculated their root mean square deviations. The along-track integrated transport uncertainties thus obtained are reported in Fig. 9. Observing that the differences between the L-ADCP and geostrophic estimates always fall within the error bars, we use the geostrophic estimates when quoting transport values below.

From Fig. 9, the full-depth transport between the Falkland Islands and South Georgia is 129 ± 21 Sv. Thus most of the transport through Drake Passage (e.g., 117 ± 15 Sv to 144 ± 6 Sv estimated by Whitworth et al. 1982; 141 ± 3 Sv estimated by MacDonald 1998) crosses the North Scotia Ridge toward the Argentine and Georgia Basin. This amount represents the contributions of the PF and SAF. In Fig. 9, the absence of any significant depression around 39°W in the curves confirms that the SACCF loop in the western Georgia Basin was hardly touched by the hydrographic line. The three-branch character of the flow described from Fig. 5 stands out again in the transport curves. The SAF, to the west of 52°W, has a transport of 52 ± 6 Sv, a value only slightly higher than the bottom-referenced estimate of 47 Sv in Drake Passage by Peterson (1992). This amount is expected to cross the North Scotia Ridge at

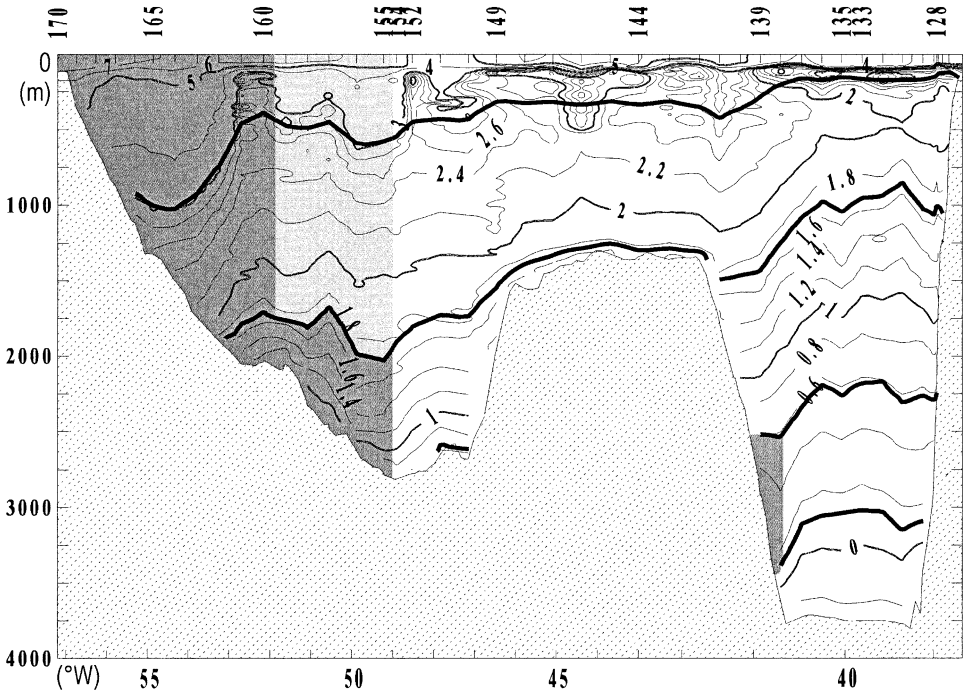

FIG. 10. Vertical section of potential temperature with the water mass isopycnal limits superimposed, showing the domains that feed the Falkland Current (dark shading), and the UCDW and AAIW regions (light shading) that might also contribute to it.

the 2000-m-deep passage to the east of Burdwood Bank (Fig. 7). The PF branch 2 in Fig. 7 has a transport of 44 ± 9 Sv from 48° to 51°W, comparable to the 45 ± 9 Sv of branch 5 from 40°15′W to 42°W. If we subtract the recirculating component around the Maurice Ewing Bank (21 ± 10 Sv), however, the net transport of branch 5 reduces to about 24 Sv, clearly lower than that of branch 2. During the ALBATROSS cruise, therefore, the PF branch over the Falkland Plateau was significantly more intense than the one along the southern slope of the Maurice Ewing Bank. Adding the net transports of the two PF branches amounts to 68 ± 10 Sv, an approximation for the magnitude of the PF in the Scotia Sea and the throughflow at Shag Rocks Passage. Finally, the net transport of 14 ± 11 Sv to the east of 40°15′W should be ascribed to water from the poleward side of the PF in the Scotia Sea that was shallow enough (<2000 m) to flow over the North Scotia Ridge to the east of Shag Rocks Passage.

6. Discussion

We focus this discussion on two topics. First, we compare the structure and transports of the equatorward flow over the Falkland Plateau with those of the Falkland Current as sampled approximately 300 km downstream by the southern end of the WOCE line A17 (Fig. 1). Second, we examine whether the southward entrainment of NADW that we observed over the eastern side of the Falkland Plateau is significant for the large-scale injection of NADW in the Antarctic Circumpolar Current.

a. Supply to the Falkland Current

In the vertical section of temperature of Fig. 10, the dark shading identifies the water that undoubtedly feeds the Falkland Current. The light shading shows water that we think may contribute to this current, but without certainty. The analyses of Peterson and Whitworth (1989) and Peterson (1992) show that the waters that are inshore of the SAF fall under the first category. The SAF, however, can only supply water from the AAIW, UCDW, and LCDW-1 layers, and the presence of denser water in the Falkland Current was noted by Peterson and Whitworth (1989). These dense components of the boundary current are visible in Fig. 11, adapted from Arhan et al. (1999), which shows the density distribution across the Falkland Current from the WOCE A17 section. In this figure, a shoreward thickening of isopycnal layers indicates a vertical sequence of deep westward velocity cores in the LCDW-1, LCDW-2, SPDW, and WSDW layers. As mentioned in section 2, the isopycnic boundary between LCDW-1 and LCDW-2 also separates two cores of high velocities against the Falkland Escarpment. Having observed in Figs. 2 and 5 that the two cores correspond to densities present in the deepest parts of the SAF and PF branch 2, respectively, the original cause of their formation probably resides in the

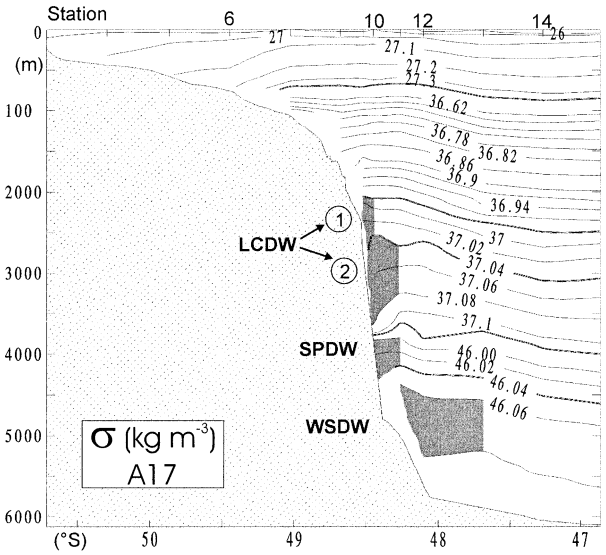

FIG. 11. (Adapted from Arhan et al. 1999.) Vertical distribution of density (σ_0, σ_2, σ_4) in the southernmost part of the WOCE line A17 (see Fig. 1), showing the different deep components of the Falkland Current against the Falkland Escarpment (shaded). The bold isopycnals show the interfaces between the water mass layers defined in Table 1.

different locations at which the SAF and the PF cross the North Scotia Ridge (Fig. 7). While the core of WSDW in the deep Falkland Current (Fig. 11) contains mostly water that has already recirculated in the Argentine Basin (Reid et al. 1977), those of SPDW and LCDW above it are formed of water that has just entered this basin. The sharp vertical density gradient at $\sigma_2 = 37.11$ (equivalent to $\sigma_4 = 45.98$) against the escarpment separates the water that has overflowed the plateau (LCDW-2) from the water that has skirted the Maurice Ewing Bank (SPDW). We noted above that this density was observed over the Falkland Plateau sill at the bottom of the PF branch number 2. This necessarily places the eastern limit of the overflow contribution to the Falkland Current at the eastern boundary of this PF branch (49°W) in the LCDW (dark shading in Fig. 10).

Unlike the LCDW layer, there is no definite reason why the longitudinal band 49°–52°W in the UCDW or AAIW should contribute to the Falkland Current. The columnar shape of the PF branch 2, particularly up to the middle of the UCDW layer, suggests a barotropic behavior and a northwestward turning of the UCDW part of the branch, similar to that of the LCDW part. In the AAIW density range, Piola and Gordon (1989) observed water from the poleward side of the SAF (the so-called Polar Frontal Zone) in the center of the cyclonic loop formed by the Falkland Current and its return flow in the Argentine Basin. This pleads in favor of an advection of water from the Polar Frontal Zone alongside the SAF in the Falkland Current. However, the bathymetric guidance is probably less efficient for the UCDW and AAIW classes of the PF branch 2 than for the LCDW part. Davis et al. (1996, their Plate 1b) presented subsurface float trajectories from depth 750 m in the same region, that seem to define two main pathways across the Falkland Plateau. One near 54°W belongs to the dark-shaded domain of Fig. 10, while the other, near 52°W, could be more representative of the light-shaded area. While the floats of the first group proceed northward along the track of the SAF, those of the second group have trajectories that turn sharply eastward above the Falkland Escarpment. These observations in the upper part of the UCDW are suggestive of a further (vertical) subdivision of the PF branch 2.

In the first line of Table 2 we report the volume transports that should contribute to the Falkland Current. Since we cannot be certain of the fate of the light-shaded water in Fig. 10, we indicate its possible additional contribution with parentheses. The second line of the same table shows the breakdown of the Falkland Current transport in water mass layers, as deduced from a hydrographic inversion of the WOCE line A17 (Wienders et al. 2000). Ignoring the WSDW contribution to the Falkland Current, which we have no means of estimating from the ALBATROSS data, the two transport values given for each water mass are compatible within the uncertainty levels. Due to differences of about 6 Sv in the AAIW and LCDW, however, the Falkland Current transport of 53.5 Sv (WSDW excluded) is nearly 10 Sv lower than the one inferred from the ALBATROSS data (63 Sv). While such a difference could be ascribed to temporal variability or estimation errors, the relative low value of the Falkland Current transport suggests that the UCDW and AAIW fractions of the PF branch 2 were not contributing to the Falkland Current at the time of WOCE A17. Other estimations of the Falkland Current transport have led to values significantly higher than the WOCE A17 one. As an example, Peterson (1992) found 88 Sv at 46°S. From the above analysis, a temporal variability of the contribution of the PF branch 2, either from the LCDW layer or through intermittent UCDW

TABLE 2. First line: Transport (Sv) per water mass over the Falkland Plateau and in the Georgia Basin (SPDW) expected to feed the Falkland Current. The values within parentheses of the AAIW and UCDW transports are the possible additional contributions of the light-shaded area in Fig. 10. Second line: Breakdown of the Falkland Current transport according to water masses deduced from an inversion of the WOCE line A17 (Wienders et al. 2000).

	AAIW	UCDW	LCDW	SPDW	WSDW	Total
ALBATROSS	35 ± 3 (5 ± 1)	15 ± 3 (20 ± 4)	12 ± 3	1.6 ± 0.5		63 ± 10
A17 (Falkland Current)	29	17	6.5	1	11	64.5 ± 10

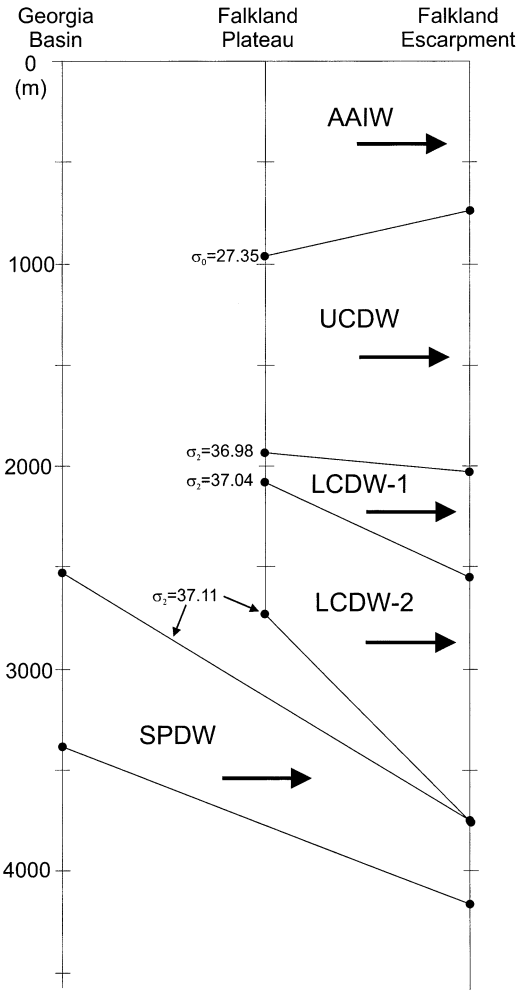

FIG. 12. Schematic representation of the depth and thickness changes experienced by the water mass layers from the Falkland Plateau and Georgia Basin to the Falkland Escarpment. The arrows show the flow direction.

or AAIW supply, is a potential cause for such variations. Model simulations have shown that there is a high correlation between the transport of the Falkland Current and that of the Antarctic Circumpolar Current in Drake Passage (Stevens and Thompson 1994). Our results suggest that a time-dependent supply of the Falkland Current by the PF northbound branch could be a link between the transport variability in the passage and that of the boundary current.

As previously described at other oceanic overflow locations (e.g., Price and O'Neil Baringer 1994), a part of the Southern Ocean water that enters the Argentine Basin over the Falkland Plateau sinks downstream of the bathymetric sill. This is readily seen from a comparison of Figs. 2 and 11 but, for more clarity, we schematically represent (Fig. 12) the depth and thickness changes experienced by the isopycnal layers from the Falkland Plateau line or the Georgia Basin line (for the SPDW) to the location of the WOCE A17 sampling at the Falkland Escarpment. Assuming that the water observed above the plateau or skirting the Maurice Ewing Bank follows alongslope trajectories, the WOCE A17 isopycnal depths reported in Fig. 12 are the most inshore ones. Momentarily disregarding the SPDW, we observe that, among the water masses overflowing the plateau, the AAIW is the only one whose thickness decreases (by about 200 m) from the ALBATROSS to the WOCE A17 sampling. The significant thickness increase of the other layers (up to 550 m for the LCDW-2) results in a sinking of the densest overflow water by about 1000 m. Although a dynamical description of the overflow is beyond the scope of this study, we note that the different behaviors of the AAIW and the other water masses might be related, through the volume conservation constraint, to a wider continental shelf along WOCE A17 than along the ALBATROSS line (Fig. 1) and, conversely, to a downstream steepening of the continental slope at deeper levels. The SPDW shows a particular behavior in that it sinks by about 1000 m on its way from the Georgia Basin to WOCE A17, and at the same time gets thinner by nearly 500 m. Such a weakening of the core of SPDW along the Falkland Escarpment, already recognized by Arhan et al. (1999), could be indicative of a partial separation of this water mass from the bathymetric slope.

b. Injection of NADW in the Antarctic Circumpolar Current

The transfer of NADW to the Antarctic Circumpolar Current, which further distributes it to the other oceanic basins, is an important component of the global thermohaline circulation. As mentioned in the introduction, our region of study is potentially important for this process, owing to the northward loop of the circumpolar current in the southwestern Argentine Basin. The presence of a NADW component in the return flow of the Falkland Current (Peterson and Whitworth 1989) reveals that a penetration of northern water into the SAF occurs at their first encounter at the Brazil–Falkland confluence. Farther downstream, at the Greenwich meridian, Whitworth and Nowlin (1987) noted that the NADW influence has progressed poleward beyond the location of the PF. In the above analysis, we described an anticyclonic flow of deep water around the Maurice Ewing Bank and observed a southward entrainment of diluted NADW by this flow. As the NADW influence is observed within the PF branch 5 over the southeastern flank of the bank, the deep anticyclonic flow appears to drive a transfer of the northern water from the SAF to the PF. Its effect might not be of much significance, however, as we noted (Fig. 8) that the salinity maximum in the LCDW-1 at the southeastern edge of the bank is barely higher than the maximum values in Drake Passage. In order to assess the importance of this mechanism at the large scale, we show in Fig. 13 the meridional distributions of the LCDW maximum salinity at

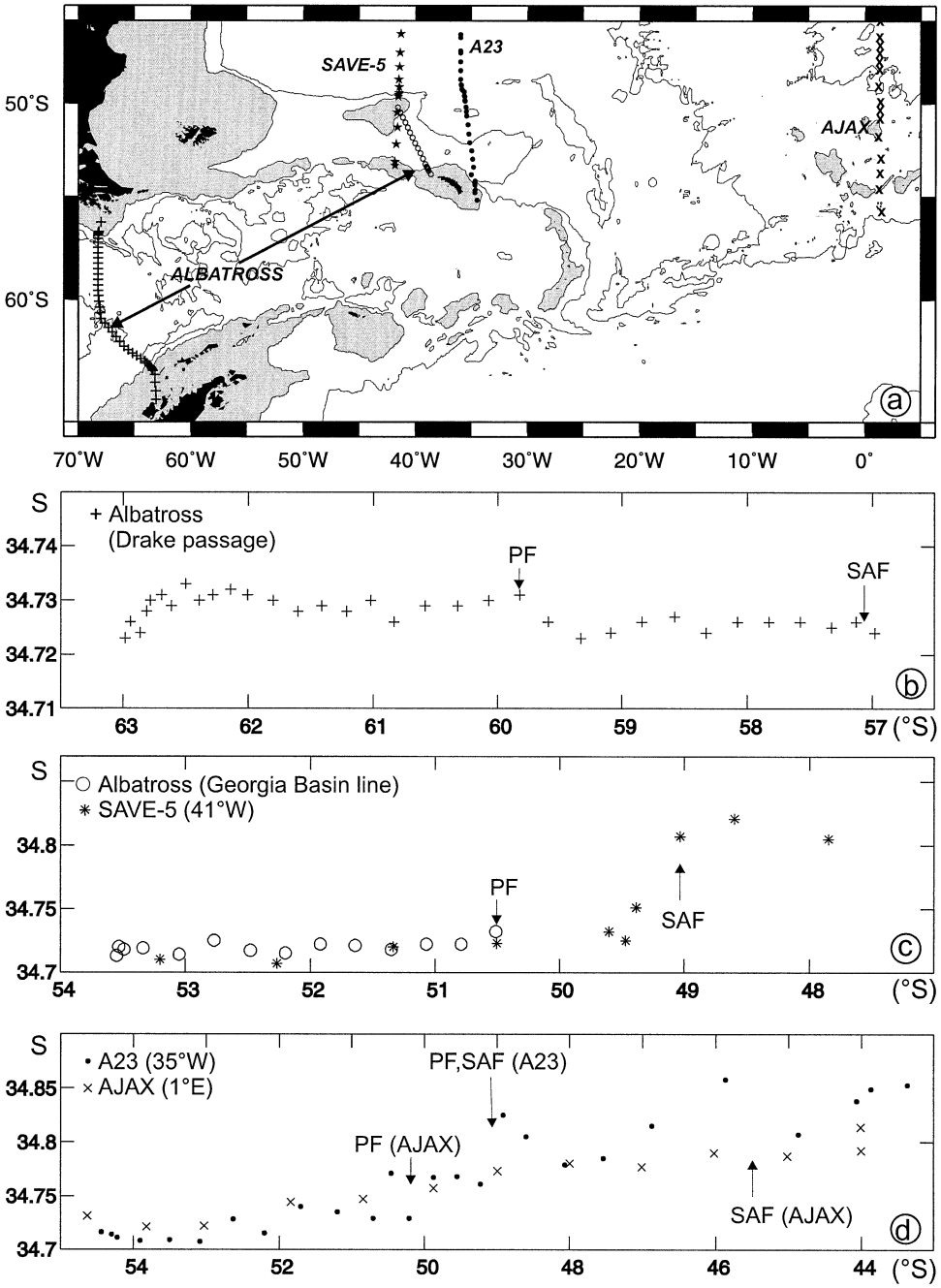

FIG. 13. (a) Map showing the locations of the hydrographic sections used in (b), (c), and (d). Isobaths 2000 m and 4000 m are shown, with a shading of the domain shallower than 2000 m. (b) Meridional distribution of the LCDW salinity maximum across Drake Passage (ALBATROSS cruise). (c) LCDW salinity maximum to the south and north of the Maurice Ewing Bank, from the ALBATROSS (circles) and SAVE-5 (stars) cruises. (d) LCDW salinity maximum near 35°W at the eastern limit of the western Georgia Basin from the WOCE A23 cruise (dots), and along the Greenwich Meridian (AJAX cruise). Note the different scales used in (b), (c), and (d).

five intersections of the circumpolar current between Drake Passage and the Greenwich meridian. The Drake Passage values (Fig. 13b) are from the ALBATROSS sampling. Two lines intersected the western Georgia Basin to the south of the Maurice Ewing Bank (Fig. 13c): The ALBATROSS Georgia Basin line used in this study, and a meridional section carried out along 41°W during cruise of 5 of the South Atlantic Ventilation Experiment (SAVE-5), of which we also show a few stations farther north to depict the SAF. Finally, in Fig. 13d, we report

the values from the WOCE line A23 along the nominal longitude 35°W, which may be regarded as the eastern limit of the western Georgia Basin, and those of the AJAX line along the Greenwich meridian (Whitworth and Nowlin 1987).

The LCDW maximum salinity in Drake Passage is 34.733 psu near 62°S (Fig. 13b). Along the Georgia Basin line the vertical maxima are generally lower than 34.72, but rise to 34.732 psu against the slope of the bank. As already noted from Fig. 8, it is not so much the difference from the Drake Passage values as the obvious entrainment of NADW in the anticyclonic flow over the Falkland Plateau that compels one to regard these higher salinities as influenced by NADW. The SAVE-5 line, despite having a coarser meridional resolution than the ALBATROSS line (Fig. 13c), sampled the saline core at a station 2640 m deep over the southern slope of the bank. The weak salinity maximum at this location (34.723 psu) relative to values to the north of the SAF (>34.8) confirms the weak role of the flow around the Maurice Ewing Bank for the poleward transfer of salinity. As already pointed out by Whitworth and Nowlin (1987), salinity maxima of about 34.75 psu (i.e., well above the Drake Passage values) are found near the PF at the Greenwich meridian (Fig. 13d). The WOCE A23 sampling, though located more than 2500 km upstream of the AJAX one, has similar values to the south of the PF, an indication that an efficient poleward transfer of NADW across the fronts of the Antarctic Circumpolar Current takes place just east of our region of study, in the western Georgia Basin. Two factors analyzed by Peterson and Whitworth (1989) and Whitworth et al. (1991) should favor this transfer. One is the close proximity of the SAF and PF (more specifically our PF branch 5) between about 40° and 35°W. The other factor is an important southward meandering of the paired fronts, possibly associated with eddy detachment, that takes place in the same longitude band.

7. Summary

We have described the structure, and quantified the transports, of the flow of southern waters between the Falkland Islands and South Georgia. In addition to the transport associated with the SAF (52 ± 6 Sv) on the western side of the Falkland Plateau, another intense columnar current (44 ± 9 Sv) exists right above the sill of the plateau that we regard as a western branch of the PF. The most prominent hydrographic signatures of the PF, however, are observed in an eastbound branch above the southeastern flank of the Maurice Ewing Bank. The transport of 45 ± 9 Sv by this branch includes a deep anticyclonic circulation around the bathymetry (21 ± 10 Sv), which locally reinforces it. The net northward transport of 129 ± 21 Sv between the Falkland Islands and South Georgia is compatible with the ~140 Sv estimates of the Drake Passage transport, given the presence of the two major fronts of the circumpolar current in the sampled region.

Focusing on the fraction of the flow that is expected to feed the Falkland Current, a value of 63 ± 10 Sv is found by adding the deep part (LCDW) of the northbound branch of the PF to the SAF transport. A possible additional contribution (up to ~25 Sv) from the UCDW and AAIW layers, if not permanent, might be a partial explanation for the large range of Falkland Current transport estimates (typically 50 Sv–100 Sv) in the literature. Ignoring this uncertain contribution, the transport breakdown according to water masses is comparable to the one in the Falkland Current across the WOCE line A17 some 300 km downstream.

The Falkland Plateau has fundamentally different effects on the SAF and the PF. As the SAF encounters the ~2800 m deep plateau downstream of the 2000-m-deep passage to the east of Burdwood Bank, it merely follows the 2000-m isobath on the western side of the plateau, without experiencing any structural alteration. In contrast, the PF, which crosses the North Scotia Ridge at the ~3200 m deep Shag Rocks Passage, is deeper than the plateau sill on its upstream side. This apparently results in a partitioning of the front in two major branches. The effect of the Falkland Plateau on the Antarctic Circumpolar Current may then be summarized as occuring in two stages. First, there is a splitting of the PF, probably in response to the divergence of isobaths 2500–3000 m on the southern side of the plateau. The resulting northbound branch crosses the plateau some 250 km to the east of the SAF. In the second stage, the deep part (LCDW) of this branch merges with the SAF on the downstream side of the plateau, where a convergence of isobaths 2000–3000 m is observed. The net result is a transfer of roughly 10 Sv (possibly more if some UCDW or AAIW accompanies the transferred LCDW) from the PF to the SAF. The adjoining denser waters position themselves below the original SAF waters against the Falkland Escarpment, thus adding a deep velocity core to the boundary current.

We have information on the fate of the LCDW core of the Falkland Current in the Argentine Basin. The presence of a velocity maximum at depth 3000–4000 m in the Falkland Return Current (Arhan et al. 1999, their Fig. 6) shows that a part of the deep core survives the current retroflection at the Brazil–Falkland confluence, thus appearing definitely locked to the SAF and the Antarctic Circumpolar Current system. Another fraction, however, proceeds equatorward along the South American continental slope and contributes (along with the WSDW) to the supply of the Atlantic Ocean by southern bottom water. Zemba (1991) estimated a transport of 5.9 Sv for this abyssal northward boundary current at 36°S, a location just to the north of the Brazil–Falkland confluence, and Speer and Zenk (1993) found a 60% contribution of LCDW to the ~4 Sv throughflow of bottom water into the Brazil Basin at the Vema Channel. When analyzing the processes that

lead to the transfer of this LCDW to subtropical latitudes, the splitting of the PF and the subsequent adjunction of some of this water to the Falkland Current, as described in this study, appear as an important first stage before the eventual partial escape from the circumpolar current system at the Falkland–Brazil confluence. Considering the transfer of northern water to the Southern Ocean, we provided evidence that an anticyclonic circulation around the Maurice Ewing Bank entrains some NADW poleward from the SAF to the southernmost branch of the PF. However, when viewed at a larger scale, this process has a negligible contribution to the injection of NADW into the circumpolar current. The meandering of the SAF and PF in the western Georgia Basin revealed by previous studies could be a more efficient mechanism.

Acknowledgments. The ALBATROSS project was funded by the U.K. Natural Environment Research Council Grant GR3/11654. MA warmly thanks his colleagues of UEA for their invitation to participate in the project. His contribution to the analysis of the data was supported by IFREMER (Grant 210161). The authors are indebted to Elaine McDonagh and Richard Sanders who were in charge of the ALBATROSS L-ADCP and nutrients work, respectively. They are grateful to two anonymous reviewers whose suggestions and detailed comments helped them improve the manuscript. The aid of Ph. Le Bot for the preparation of the figures is acknowledged.

REFERENCES

Arhan, M., K. J. Heywood, and B. A. King, 1999: The deep waters from the Southern Ocean at the entry to the Argentine Basin. *Deep-Sea Res. II,* **46,** 475–499.

Broecker, W. S., and Coauthors, 1998: How much deep water is formed in the Southern Ocean? *J. Geophys. Res.,* **103,** 15 833–15 843.

Davis, R. E., P. D. Killworth, and J. R. Blundell, 1996: Comparison of autonomous Lagrangian circulation explorer and fine resolution Antarctic model results in the South Atlantic. *J. Geophys. Res.,* **101** (C1), 855–884.

Durrieu de Madron, X., and G. L. Weatherly, 1994: Circulation, transport, and bottom boundary layers of the deep currents in the Brazil Basin. *J. Mar. Res.,* **52,** 583–638.

Egbert, G. D., A. F. Bennett, and M. G. G. Foreman, 1994: TOPEX/POSEIDON tides estimated using a global inverse model. *J. Geophys. Res.,* **99** (C12), 24 821–24 852.

Georgi, D. T., 1981: Circulation of bottom waters in the southwestern South Atlantic. *Deep-Sea Res.,* **28A,** 959–979.

Gordon, A. L., D. T. Georgi, and H. W. Taylor, 1977: Antarctic Polar Front zone in the western Scotia Sea—Summer 1975. *J. Phys. Oceanogr.,* **7,** 309–328.

Heywood, K. J., and D. P. Stevens, 2000: ALBATROSS cruise report. UEA Cruise Rep. Series No. 6, 62 pp.

MacDonald, A. M., 1998: The global ocean circulation: A hydrographic estimate and regional analysis. *Progress in Oceanography,* Vol. 41, Pergamon, 281–382.

Moore, J. K., M. R. Abbott, and J. G. Richman, 1997: Variability in the location of the Antarctic Polar Front (90°−20°W) from satellite sea surface temperature data. *J. Geophys. Res.,* **102** (C13), 27 825–27 833.

Naveira Garabato, A. C., K. J. Heywood, and D. P. Stevens, 2002: Modification and pathways of Southern Ocean deep waters in the Scotia Sea. *Deep-Sea Res. I,* **49,** 681–705.

Orsi, A. H., W. D. Nowlin, and T. Whitworth, 1993: On the circulation and stratification of the Weddell Gyre. *Deep-Sea Res. I,* **40,** 169–203.

——, T. Whitworth, and W. D. Nowlin, 1995: On the meridional extent and fronts of the Antarctic Circumpolar Current. *Deep-Sea Res. I,* **42,** 641–673.

Peterson, R. G., 1992: The boundary currents in the western Argentine Basin. *Deep-Sea Res.,* **39,** 623–644.

——, and T. Whitworth, 1989: The Subantarctic and Polar Fronts in relation to deep water masses through the Southwestern Atlantic. *J. Geophys. Res.,* **94** (C8), 10 817–10 838.

Piola, A. R., and A. L. Gordon, 1989: Intermediate waters in the southwest South Atlantic. *Deep-Sea Res.,* **36,** 1–16.

Price, J. F., and M. O'Neil Baringer, 1994: Outflows and deep water production by marginal seas. *Progress in Oceanography,* Vol. 33, Pergamon, 161–200.

Reid, J. L., W. D. Nowlin, and W. C. Patzert, 1977: On the characteristics and circulation of the southwestern Atlantic Ocean. *J. Phys. Oceanogr.,* **7,** 62–91.

Sievers, H. A., and W. D. Nowlin, 1984: The stratification and water masses at Drake Passage. *J. Geophys. Res.,* **89** (C6), 10 489–10 514.

Sparrow, M. D., K. J. Heywood, J. Brown, and D. P. Stevens, 1996: Current structure of the south Indian Ocean. *J. Geophys. Res.,* **101,** 6377–6391.

Speer, K. G., and W. Zenk, 1993: The flow of Antarctic Bottom Water into the Brazil Basin. *J. Phys. Oceanogr.,* **23,** 2667–2682.

Stevens, D. P., and S. R. Thompson, 1994: The South Atlantic in the Fine Resolution Antarctic Model. *Ann. Geophys.,* **12,** 826–839.

Thorpe, S. E., K. J. Heywood, M. A. Brandon, and D. P. Stevens, 2001: Variability of the Southern Antarctic Circumpolar Current Front north of South Georgia. *J. Mar. Syst.,* submitted.

Trathan, P. N., M. A. Brandon, E. J. Murphy, and S. E. Thorpe, 2000: Transport and structure within the Antarctic Circumpolar Current to the north of South Georgia. *Geophys. Res. Lett.,* **27,** 1727–1730.

Warren, B. A., 1969: Divergence of isobaths as a cause of current branching. *Deep-Sea Res.,* **16** (Suppl.), 339–355.

Whitworth, T., and W. D. Nowlin, 1987: Water masses and currents of the Southern Ocean at the Greenwich meridian. *J. Geophys. Res.,* **92** (C6), 6462–6476.

——, ——, and S. J. Worley, 1982: The net transport of the Antarctic circumpolar current through Drake Passage. *J. Phys. Oceanogr.,* **12,** 960–971.

——, ——, R. D. Pillsbury, M. I. Moore, and R. F. Weiss, 1991: Observations of the Antarctic circumpolar current and deep boundary current in the Southwest Atlantic. *J. Geophys. Res.,* **96** (C8), 15 105–15 118.

Wienders, N., M. Arhan, and H. Mercier, 2000: Circulation at the western boundary of the South and equatorial Atlantic: Exchanges with the ocean interior. *J. Mar. Res.,* **58,** 1007–1039.

Zemba, J. C., 1991: The structure and transport of the Brazil Current between 27° and 36° south. Ph.D. thesis, Massachusetts Institution of Technololgy–Woods Hole Oceanographic Institution, 160 pp.